Numerical Investigation of an Active Jet Control Method for Hypersonic Inlet Restart

JIN Yichao[1,2], *YAO Wei*[2,3*]

1. Institute of Applied Physics and Computational Mathematics, Beijing 100094, P.R. China; 2. Key Laboratory of High-Temperature Gas Dynamics, Institute of Mechanics, Chinese Academy of Sciences, Beijing 100190, P.R. China; 3. School of Engineering Science, University of Chinese Academy of Sciences, Beijing 100049, P.R. China

(Received 25 October 2022; revised 7 December 2022; accepted 13 December 2022)

Abstract: A flow control method based on an active jet is developed to restart hypersonic inlets. The dynamic restarting process is numerically reproduced by unsteady Reynolds averaged Navier-Stokes (RANS) modeling to verify the effectiveness and reveal the influence of jet conditions. The active jet improves the inlet unstart status by drawing the high-pressure separation bubble from the internal compression duct and performing a full expansion to alleviate the adverse pressure gradient. Moreover, the favorable pressure gradient in the inlet caused by jet expansion allows for a successful restart after turning off the jet. The influence of the jet momentum ratio is then analyzed to guide the design of the active jet control method and choose the proper momentum ratios. A low jet momentum does not eliminate the high-pressure separation bubble, whereas an excessive jet momentum causes severe momentum loss due to the induced shock. The general rule in restarting the inlet using an active jet is to allow a full jet expansion downstream of the jet slot while avoiding excessive momentum loss upstream and preventing the thick low-speed layer.

Key words: hypersonic inlet; unstart; restart; active jet; flow control

CLC number: O354 **Document code**: A **Article ID**: 1005-1120(2022)06-0651-12

0 Introduction

Hypersonic inlets are vital components for scramjet engines in high-speed air-breathing vehicles. In the unstart hypersonic inlet, the interaction caused by the strong shock wave/boundary layer leads to a considerable decrease in the compression efficiency and flow-capture capability, as well as a higher aerodynamic drag[1], which seriously reduces the flight quality of the aircraft and even leads to flight failure. Thus, good starting capabilities are crucial for the stable and efficient operation of hypersonic vehicles.

Over the past decades, numerous studies have been conducted on the start performance of hypersonic inlets, including the unstart mechanism[2-3], unstart detection[4-5], and flow control[6-9]. For better flight performance, various control methods have been developed to prevent or delay its unstart, e.g., bleeding[10], vortex generators[11-12], boundary layer blowing[13], and energy addition[14]. The general idea behind these methods is to either remove low momentum flow away from the wall or increase the boundary layer's momentum.

In addition to suppressing unstart, improving the restart capability of hypersonic inlets is also an important issue. The self-start performance of fixed-geometry inlets can be characterized by the self-start limit theories[15-16]. For the inlet with a weak self-start ability, variable geometry and suction devices are commonly used to assist in restarting. Falempin et al.[17] adapted the translating cowl to vary the contraction ratio in the Mach number ranging from 2 to 8. Dalle et al.[18] used both moving and rotating cowl to adjust the contraction ratio and found that the variable-geometry inlet performs better in the wide

*Corresponding author, E-mail address: weiyao@imech.ac.cn.

How to cite this article: JIN Yichao, YAO Wei. Numerical investigation of an active jet control method for hypersonic inlet restart[J]. Transactions of Nanjing University of Aeronautics and Astronautics, 2022, 39(6): 651-662.

http://dx.doi.org/10.16356/j.1005-1120.2022.06.002

Mach range. Teng and Yuan[19] implemented a variable-geometry cowl sidewall and effectively restarted the inlet from an unstart status. Liu et al.[20] dynamically simulated the rotating process of an inlet cowl and also successfully restarted the inlet. The variable geometry method is effective by adapting the contraction ratio with the operating condition, but it significantly increases the structure weight and control complexity and brings sealing problems[21]. An alternative method to assist the inlet restart is gas bleeding through a porthole on the inlet sidewall. Häberle and Gülhan[22] effectively controlled the lip-shock-induced separation in hypersonic inlets at Mach 6 with a mass discharge ratio of 5.5%. Yuan and Liang[23] decreased the self-starting Mach number from 4.2 to 3.4, while investigating the influence of suction position. Similar inlet restart applications of the bleeding method also have been conducted by Chang et al[24]. However, the main drawback of the bleeding method is that it may cause a significant portion of mass loss.

Active jet is a vital control technology in subsonic and supersonic flow. It has been universally used to reduce drag[25], control flow separation[26], improve flow distortion[27-29], and suppress shock oscillations[30]. The method directs the flow by introducing mass and energy into the mainstream. However, due to the existing separation region and severe adverse pressure gradient within the inlet, there have been more significant challenges for the active jet to restart the inlet, and the reports on this issue are sparse. When imposing an active jet, Van Wie et al.[31] experimentally studied the influences of steady fluid injection on unstart and restart in the supersonic inlet and described the potential mechanism. However, whether the inlet start can be sustained after turning off the active jet was not investigated. Subsequently, You[32] experimentally achieved the restart in the supersonic inlet using the active jet. He also numerically conducted detailed assessments, pointing out that alleviating the throat choking in virtue of the flow spillage caused by the jet is the key to restarting the inlet. Till now, the effectiveness of the active jet method has been validated in supersonic inlets with relatively low Mach numbers, providing the theoretical support for the auxiliary application of restarting high-speed inlets. Nevertheless, as internal contraction ratios increase, the flow separation inside the internal compression duct of the hypersonic inlet worsens, resulting in a more significant blockage to the incoming flow and, accordingly, a more difficult inlet restart. To the authors' best knowledge, rare studies have been reported to successfully apply the active jet method to restart the hypersonic inlet.

Based on these contents, this study explores the effectiveness and feasibility of the active jet method in restarting hypersonic inlets. Firstly, the dynamic restarting process when imposing an active jet was wholly reproduced by unsteady Reynolds averaged Navier-Stokes (RANS) modeling, revealing the key mechanisms in hypersonic inlet restart using an active jet. The impact of the jet momentum ratio was then examined further in this study. Finally, the general rule was summarized to provide guidelines for the design of the active jet method for restarting hypersonic inlets.

1 Physical Models and Numerical Methods

1.1 Governing equations

The three-dimensional compressible Navier-Stokes equations (NSEs) are solved for a set of conservative variables

$$\frac{\partial \rho}{\partial t}+\frac{\partial(\rho u_i)}{\partial x_i}=0 \tag{1}$$

$$\frac{\partial \rho u_i}{\partial t}+\frac{\partial(\rho u_i u_j)}{\partial x_j}=-\frac{\partial p}{\partial x_i}+\frac{\partial \tau_{ij}}{\partial x_j} \tag{2}$$

$$\frac{\partial \rho E}{\partial t}+\frac{\partial(\rho u_j H)}{\partial x_j}=\frac{\partial(u_i \tau_{ij})}{\partial x_j}-\frac{\partial}{\partial x_j}\left(\left(\frac{\mu}{Pr}+\frac{\mu_t}{Pr_t}\right)\frac{\partial T}{\partial x_j}\right) \tag{3}$$

where t denotes the time, x_i the Cartesian coordinate in the direction i, ρ the density, T the temperature, u_i the velocity component in x_i direction (spatial dimension $i=1, 2, 3$), p the pressure, and τ_{ij} the viscous stress tensor; $E=e(p, T)+0.5u_i^2$ and $H=h(p, T)+0.5u_i^2$ are the total internal energy and absolute enthalpy, respectively. The laminar

and turbulent Prandtl numbers are assumed to be 0.72 and 0.9. The laminar dynamics viscosity coefficient μ is calculated by Sutherland law, and the turbulent viscosity coefficient is computed using the turbulence model.

1.2 Turbulence model

The main purpose of this paper is to explore the effectiveness of the active jet on the inlet restart, rather than the elaborate simulation of complex flows. Therefore, the more computationally-efficient RANS approach is applied in the present study. The two-equation shear stress transport (SST) turbulence model, developed by Menter[33] is adopted in the present paper to solve the turbulent fluctuations. The two transport equations of k-ω SST model are described below

$$\frac{\partial(\rho k)}{\partial t}+\frac{\partial(\rho u_j k)}{\partial x_j}=\frac{\partial}{\partial x_j}\left[(\mu+\sigma_k\mu_t)\frac{\partial k}{\partial x_j}\right]+P_k-\beta^*\rho\omega k \tag{4}$$

$$\frac{\partial(\rho\omega)}{\partial t}+\frac{\partial(\rho u_j\omega)}{\partial x_j}=\frac{\partial}{\partial x_j}\left[(\mu+\sigma_\omega\mu_t)\frac{\partial \omega}{\partial x_j}\right]+P_\omega-\beta\rho\omega^2+2(1-f_1)\frac{\rho\sigma_{\omega 2}}{\omega}\frac{\partial k}{\partial x_j}\frac{\partial \omega}{\partial x_j} \tag{5}$$

where P_k and P_ω are the production terms of k and ω equations, written as

$$\begin{cases} P_k=\mu_t\Omega^2 \\ P_\omega=C_\omega\rho\Omega^2 \\ \mu_t=\dfrac{a_1\rho k}{\max(a_1\omega, f_2\|\Omega\|)} \end{cases} \tag{6}$$

where Ω is the magnitude of vorticity. A detailed description of the other model parameters can be found in Ref.[33].

1.3 Solver and numerical method

The governing equations are solved by an in-house developed finite-volume compressible RANS solver, which is extended from the open-source CFD package SU2[34]. In the present simulations, the nonlinear inviscid convective fluxes are evaluated using the Roe flux-difference scheme[35]. A second-order spatial accuracy in reconstructing primitive convective fluxes at faces is achieved by the monotone upstream-centered schemes for the conservation laws (MUSCL) method[36] with the min-mod limiter. Temporal integration is advanced by the implicit lower-upper symmetric Gauss-Seidel (LU-SGS) scheme[37]. Dual time step method[38] with LU-SGS scheme is employed in unsteady modelings. For the second-order temporal accuracy, the maximum density residual decreases about three orders of magnitude in the inner loop. A fixed physical time-step of 1.6×10^{-7} s is employed in the time-marching process.

1.4 Experimental case

Fig.1 shows the examined two-dimensional hypersonic inlet configured with two compression ramps, with the inclination angles of 9° and 14° to the freestream flow direction, respectively. An isolator is immediately behind the throat with a constant cross-section of 10 mm in height and 115 mm in length. Fig.2 schematically illustrates the computational grid and boundary conditions, which are set up by referring to Ref.[9]. The computational domain is extended by an additional expansion channel. A multi-block structured grid is utilized to mesh the whole domain. The mesh is clustered in the second ramp, internal compression duct and isolator to better capture the flow structures, while the coarser mesh is used in the far field to reduce the computational cost. To take into account the three-dimensioanl turbulence effect, the span-wise length is set to 10 mm, with the periodic boundary conditions applied on the two lateral sides.

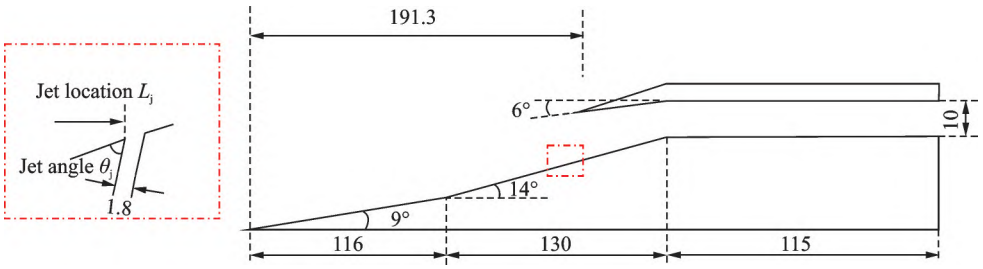

Fig.1 Two-dimensional hypersonic inlet configuration

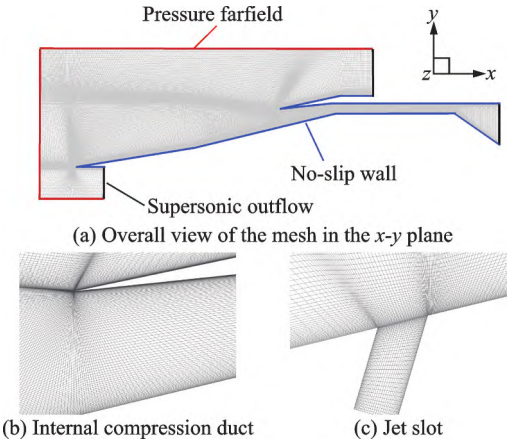

Fig.2 Schematics of the computational domain and boundary conditions

2 Correlations and Validations

2.1 Validation

The numerical framework is validated against the benchmark experiment of Häberle and Gülhan[39]. The model inlet was tested in a hypersonic tunnel with the flow conditions in Table 1.

Table 1 Flow conditions for the validation case

Parameter	Value
Mach number Ma_∞	7
Freestream pressure p_∞ / Pa	170
Freestream temperature T_∞ / K	46
Total temperature T_{t0} / K	500
Total pressure p_{t0} / Pa	0.7×10^6
Wall temperature T_w / K	300.0

From Fig.3, the flow structures, such as the separation bubble, separation-induced shock, and reflected shock waves inside the isolator, are well captured and agree with the experimental results[39]. Fig.4 compares the pressure coefficient C_p distributions along the upper and lower surfaces of the inlet, where overall good agreements have been obtained.

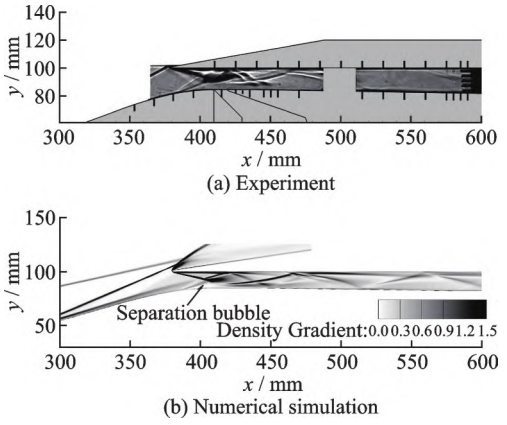

Fig.3 Schlieren images of the hypersonic inlet flow

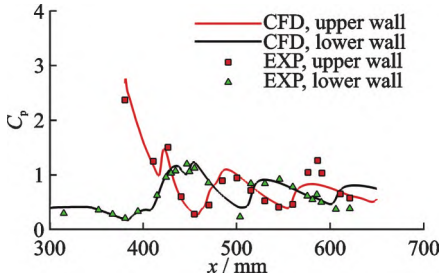

Fig.4 Simulated and measured pressure on the upper and lower walls

2.2 Grid convergence analysis

Three meshes listed in Table 2, where N_x, N_y, N_z are the grid numbers in the x, y, z directions and Δ_{min} is the height of the first layer grid, are used to verify the grid convergence for the model in Fig.1. The freestream has a Mach number of 3.5, a static pressure of 5 529.31 Pa, and a static temperature of 216.65 K. The main flow structures in the inlet were all predicted accurately by the three meshes. As compared in Fig.5, the slight difference of less than 0.5% between the three predictions indicates that the grid convergence has been achieved. In the subsequent modelings, the medium mesh will be used.

Table 2 Summary of the mesh configurations

Case	Grid resolution in inlet/isolator		Total grid
	$N_x\times N_y\times N_z$	Δ_{min} / mm	
Coarse	$300\times100\times20$	0.015	1.2×10^6
Medium	$450\times150\times25$	0.010	2.5×10^6
Fine	$540\times180\times35$	0.008	4.7×10^6

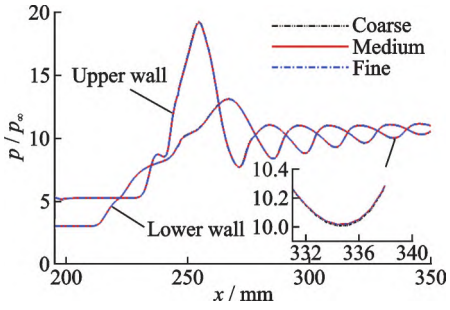

Fig.5 Wall pressure in a start status predicted by different mesh resolutions

3 Results and Discussion

Fig.6 shows the mass flow ratio Φ and total pressure recovery coefficient σ_p varying with the freestream Mach number, and the performance parameters at the inlet throat are computed as

$$\begin{cases} \tilde{\Phi} = \int \rho |V \cdot \mathrm{d}A| \\ \tilde{\Psi} = \dfrac{\int \Psi \cdot \rho |V \cdot \mathrm{d}A|}{\int \rho |V \cdot \mathrm{d}A|} \end{cases} \tag{7}$$

where $\tilde{\Phi}$ is the total mass flow rate, V the velocity, A the area element, and $\tilde{\Psi}$ the mass-weighted averaged variable, e.g., the Mach number Ma, static pressure p, or total pressure p_t. Φ is calculated by $\tilde{\Phi}/[(\rho V)_\infty A_0]$, with $(\rho V)_\infty$ denoting the freestream mass flux and A_0 the inlet windward area. σ_p is defiend as p_t/p_{t0}, with p_{t0} denoting the total pressure of freestream flow.

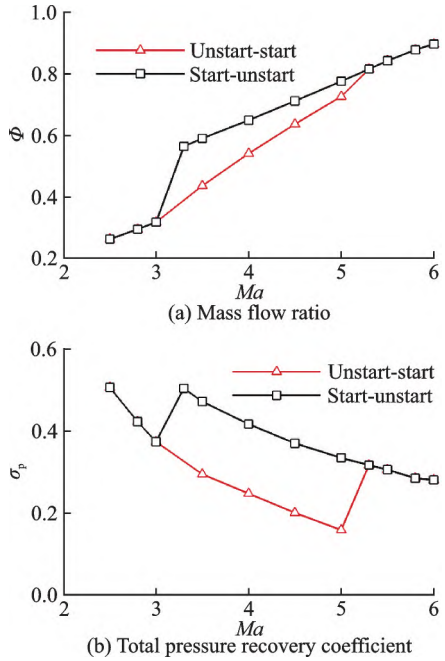

Fig.6 Throat parameters in hysteresis loops

A noticeable hysteresis phenomenon, or flow memory effect[1], was observed. As the freestream Mach number increases from 2.5 to 6, the hypersonic inlet transits from unstart to start status. However, when conversely decreasing the Mach number, the transition from start to unstart status does not follow exactly the same route. The dual routes between 3.3 and 5.3 form a well-known hysteresis loop.

Fig.7 shows the start and unstart Mach contours under the freestream Mach number of $Ma_\infty = 3.5$. The performance parameters at the throat are compared in Table 3. In an off-design condition, the external shock waves fall ahead of the inlet entrance. When the inlet starts, the reflected shock waves of the cowl shock form a shock train in the isolator to balance the upstream and downstream pressure. Under the unstart status, the separation-induced shock leads to flow spillage and momentum loss. Behind the aerodynamic throat, the incoming air is further receded to subsonic.

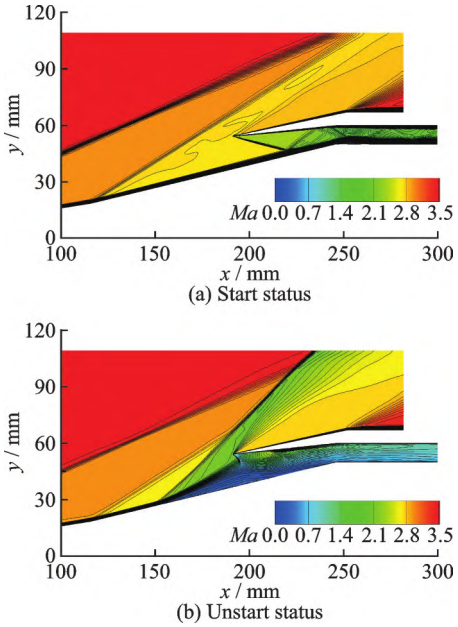

Fig.7 Mach contours under start and unstart status

Table 3 Throat parameters at Ma_∞=3.5

Parameter	Value	
	Unstart	Start
Averaged Mach number Ma_e	0.838	1.603
Averaged pressure (p_e/p_∞)	14.21	10.53
Mass flow ratio	0.44	0.59
Total pressure recovery coefficient	0.30	0.47

As shown in Fig.8, the separation-induced and lip shock combination produces a sizeable adverse pressure gradient, which is crucial to maintaining unstart status. To dispel the separation bubble, a higher flow velocity is usually needed to overcome the adverse pressure. However, it would lead to a relatively high self-starting Mach number. For bet-

ter starting capabilities, it is desired to restart the inlet without the demanding requirement for freestream conditions, e. g., using the active jet method as introduced below.

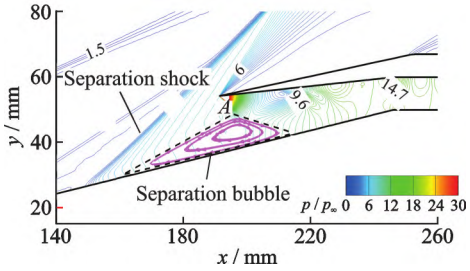

Fig.8 Flow structures of unstart status

3.1 Analysis for restart process

In this section, the effect of the active jet on restarting the inlet from an unstart status is examined. The freestream and jet parameters are summarized in Table 4. And the jet momentum ratio ($J=\rho_j u_j^2/\rho_\infty u_\infty^2$, with subscript j denoting the jet exit conditions and ∞ the freestream conditions) is set to 7.37. The main flow structures are briefly illustrated in Fig.9 for a successful restarting case when bearing an active jet.

Table 4 Summary of freestream and jet parameters

Parameter	Value
Mach number Ma_∞	3.5
Freestream pressure p_∞ / Pa	5 529.31
Freestream temperature T_∞ / K	216.65
Jet location L_j/mm	160.0
Jet angle θ_j / (°)	80

The jet issued from a slot bends into the internal compression duct and then quickly expands to be supersonic flow. Due to insufficient space and residence time, the expansion is not fully expanded. However, compared with the case without an active jet, the high-pressure separation bubble almost vanishes downstream of the jet, and the adverse pressure is remarkably alleviated. After turning off the active jet, the inlet successfully restarts and maintains a started status.

To gain a deep insight into the key flow dynamics, the transient restarting process when applying an active jet is numerically reproduced in Fig.10. At

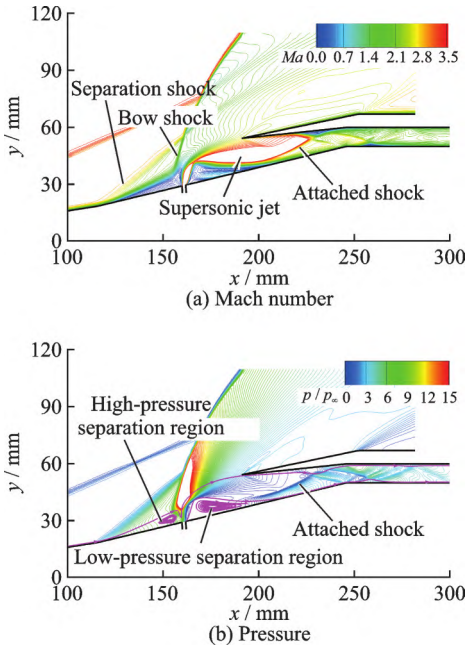

Fig.9 Flow structures with active jet

$\Delta t = 0.08$ ms, the high-speed jet acts as an aerodynamic obstacle on the lower wall, blocking the freestream air. A high-pressure separation bubble and its induced shock emerge upstream of the jet. Meanwhile, the bow shock induced by the jet results in a strong flow spillage and a significant reduction in the flow velocity. At $\Delta t = 0.26$ ms, the jet strengthens the separations in both the upstream and the downstream of the slot. The high-pressure separation bubble extends further to a far upstream of the jet. The pressure in the isolator significantly reduces, and the jet penetration depth increases. The separation bubble grows continuously and nearly entirely blocks the inlet at $\Delta t = 0.60$ ms. The pressure behind the jet decreases further. At $\Delta t = 1.12$ ms, the jet is bent by the high-momentum freestream towards the inlet and expands in the internal compression duct, which narrows the separation bubble and alleviates the adverse pressure gradient. At $\Delta t = 1.79$ ms, the low-pressure separation bubble downstream of the jet shrinks considerably, and most of the jet flow enters the inlet. A large low-pressure region is formed behind the jet when reaching steady due to the entrainment effect. The adverse pressure gradient within the inlet has been effectively alleviated and replaced by a high-pressure separation region upstream.

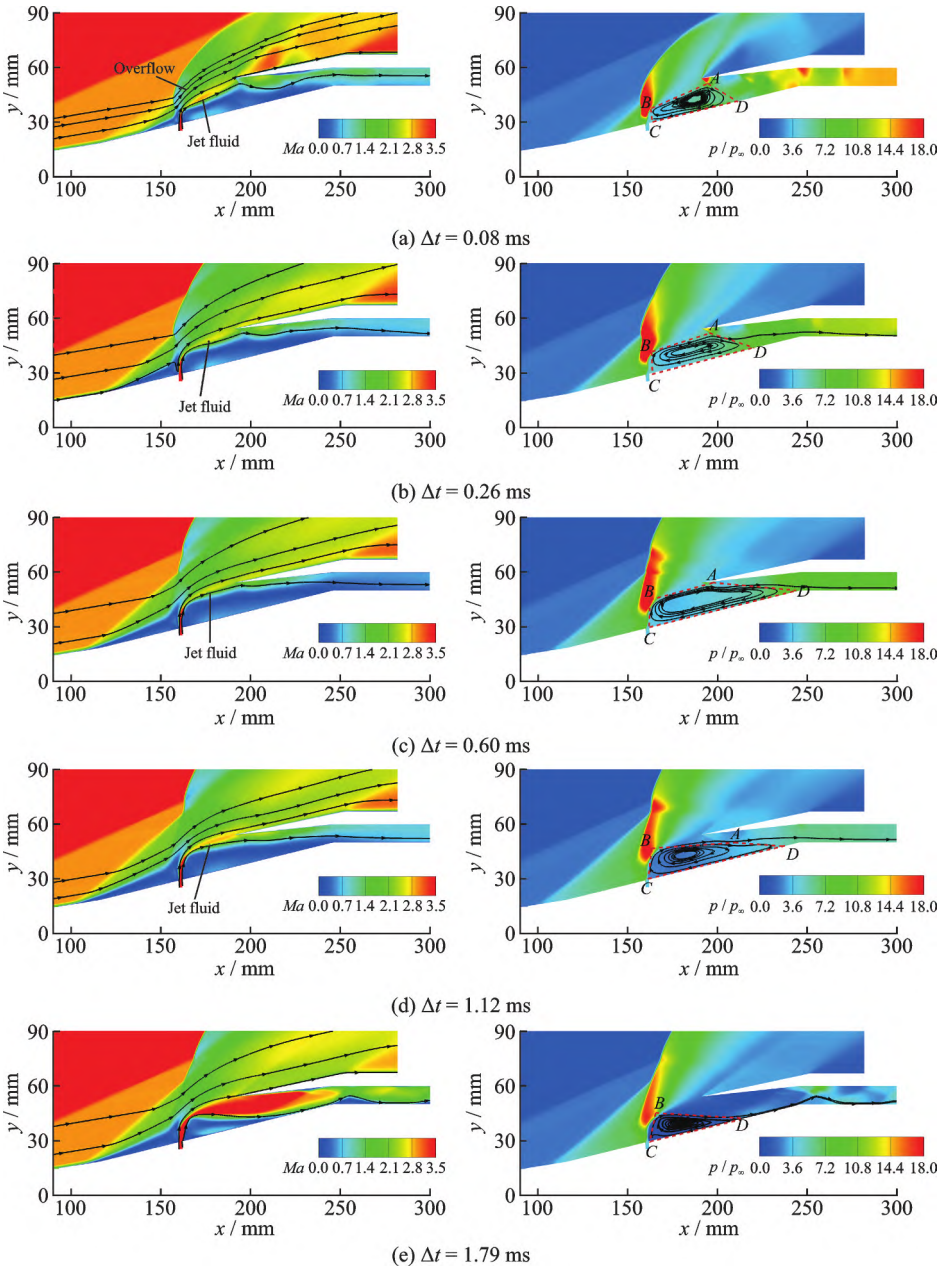

Fig.10 Evolution of Mach and pressure contours bearing an active jet

The flow evolution after turning off the active jet is shown in Fig.11. The separation bubble shrinks to the jet root and will vanish gradually, and a bow shock moves to the entrance of the internal compression duct, as seen in Fig.11(a). However, from Fig.11(b), the blocking of the high-pressure separation bubble results in a thicker low-momentum boundary layer, which lasts for a long time before its disappearance and is unfavorable for restart. During the restart process, the shock/boundary interaction produces a local high-pressure region and may even induce new separation, as shown in Fig.11(c). With the swallowing of the shock train by the internal compression duct, the supersonic incoming flow fully enters the inlet and inhibits the growth of the separation bubble. The final stable flow in Fig.11(d) indicates a start status. Thus, the start status can sustain even after the removal of the active jet. As seen, the general principle of the active jet method is to draw the high-pressure separation bubble from the internal compression duct and then inhibit the reformulation of large separation region.

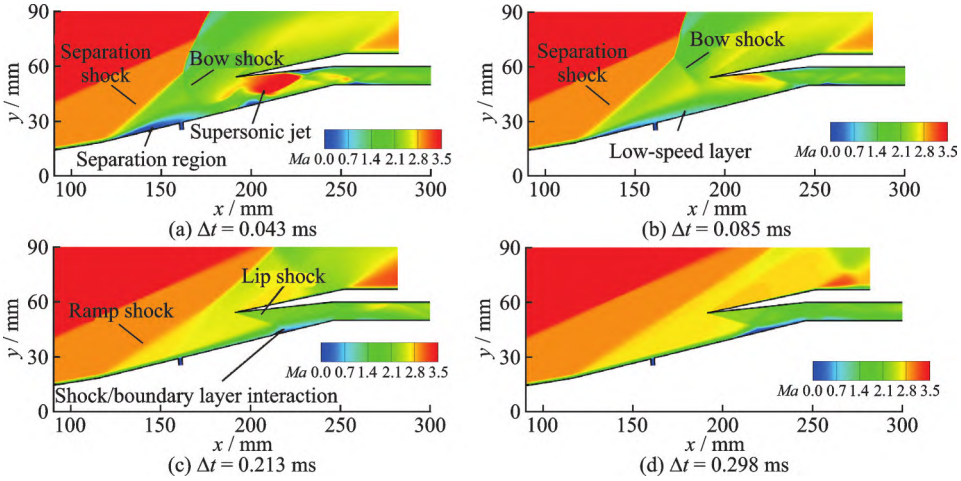

Fig.11 Evolution of Mach contours after turning off the active jet

3.2 Influence of jet momentum ratio

In this section, jet momentum ratios ranging from 3.61 to 12.64 were numerically tested. Fig.12 shows the averaged Mach number and pressure at the throat under different jet momentum ratios when the flow reaches stable. The jet momentum ratios of 5.97, 7.37, and 8.91 all successfully restarted the inlet from an unstart status. The pressure at the throat decreases monotonously from the unstart state with the increased jet momentum ratio. The averaged Mach number first increases until $J=8.91$, then decreases monotonously. Except the case with $J=3.61$, all the other cases reach supersonic at the throat.

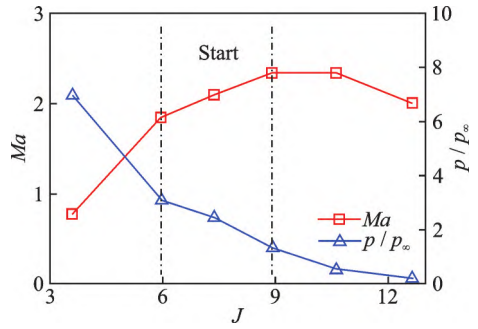

Fig.12 Throat parameters under different jet momentum ratios

Fig.13 compares the Mach contours under different jet momentum ratios. As the jet momentum ratio increases, a more remarkable increase in the jet penetration depth can be observed. At $J=3.61$, the active jet enlarges the separation bubble and aggravates the unstart. When the jet momentum ratio reaches 4.72, the inlet flow oscillates between the start and unstart statuses. Between the jet momentum ratio of 5.97 and 8.91, the jet fully blocks the incoming flow, and the jet flow nearly entirely enters the inlet, where the expansion of the jet wake effectively alleviates the adverse pressure gradient in the internal compression duct and results in a successful inlet restart after removing the jet. With the further increase of the jet momentum ratio to 10.61, the too higher jet penetration depth causes flow spillage, and it also induces giant separation bubbles close to the jet root and considerably strengthens the induced shock. In consequence, the hypersonic inlet fails to restart after the jet is turned off, as shown in Fig.14.

After turning off the jet, the separation bubble on the lower wall thickens the boundary layer and reduces the effective flow-through area, while the induced shock wave reduces the incoming flow momentum. The growth of the new separation bubble retrogresses the inlet to the unstart status. The above analysis indicates that the key to restarting the inlet is to reduce the adverse pressure gradient and prevent severely thickening the boundary layer.

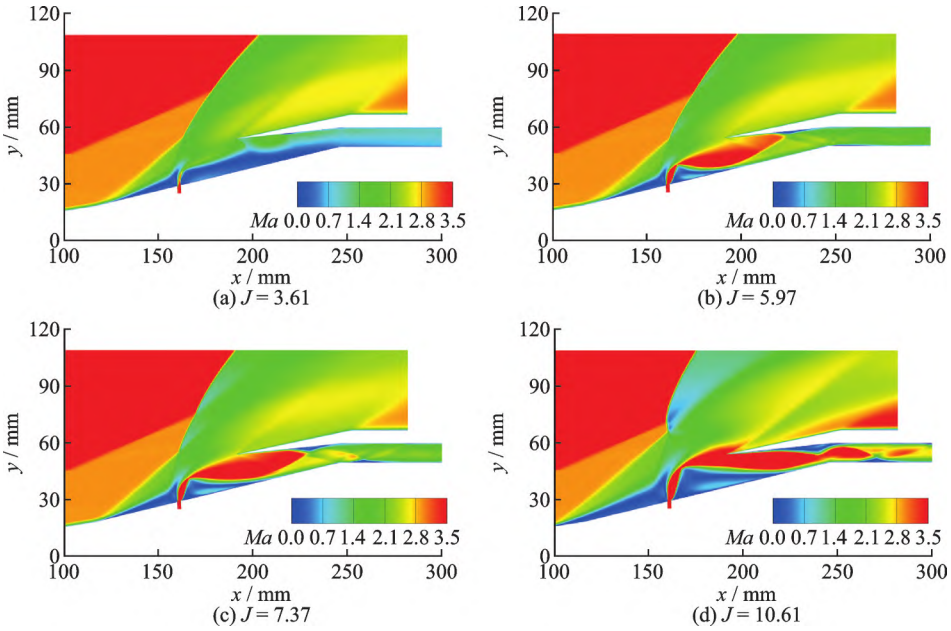

Fig.13 Mach contours under different jet momentum ratios

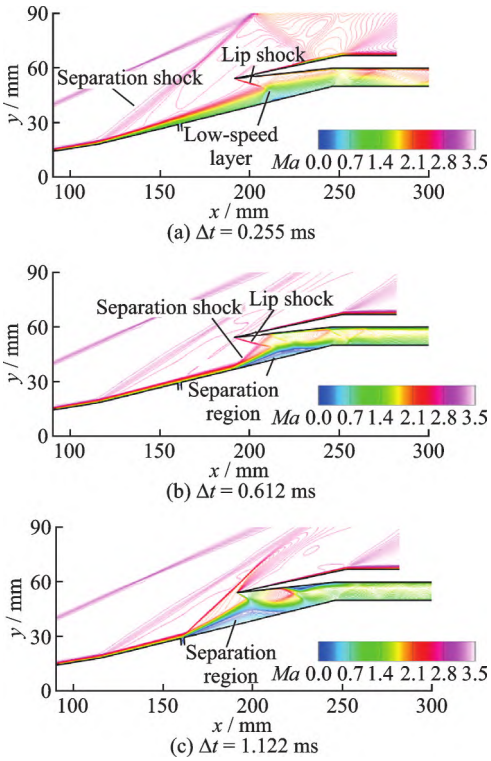

Fig.14 Evolution of flow structures at $J = 10.61$ after turning off the jet

4 Conclusions

This study presented an active flow control method based on a high-pressure jet to restart the hypersonic inlet. The dynamic restarting process was numerically reproduced to elaborate the restarting mechanism. The inlet restarting capability of the proposed active jet control method was thoroughly validated, and the restarting principle was revealed. The inlet unstart is usually caused by the strong adverse pressure gradient and the reduction in the effective flow-through area by the boundary-layer blockage effect. The high-momentum jet wake flow blocks the incoming flow and alleviates the congestion downstream. And a full expansion within the internal compression duct not only overcomes the adverse pressure gradient but also eliminates the high-pressure separation bubble. The dynamic flow evolution of a successful restart follows two main steps: Firstly, the high-pressure separation bubble is transferred upstream, then the adverse pressure gradient in the internal compression duct is alleviated by the jet expansion; secondly, the freestream enters after turning off the jet and reestablishes the start flow field from a favorable pressure gradient.

The influence of the jet momentum ratio was analyzed to guide the design of the active jet control method. The inlet can be restarted at a moderate jet momentum ratio between 5.97 and 8.91; the lower jet momentum can not effectively eliminate the adverse pressure gradient, while a higher jet momentum causes severe spillage and loss of flow momentum. When restarting the inlet with an active jet, the general rule is to allow a full jet expansion with-

in the inlet, which provides flushing and sealing effects while avoiding excessive momentum loss upstream and preventing the thick low-speed layer after turning off the active jet. This rule should be followed when optimizing jet configurations.

References

[1] CHANG J T, LI N, XU K J, et al. Recent research progress on unstart mechanism, detection and control of hypersonic inlet[J]. Progress in Aerospace Sciences, 2017, 89: 1-22.

[2] WAGNER J L, VALDIVIA A, CLEMENS N T. Experimental investigation of unstart in an inlet/isolator or model in Mach 5 flow[J]. AIAA Journal, 2009, 47(6): 1528-1542.

[3] LAURENCE S J, LIEBER D, SCHRAMM J M, et al. Incipient thermal choking and stable shock-train formation in the heat-release region of a scramjet combustor. Part Ⅰ: Shock-tunnel experiments[J]. Combustion and Flame, 2015, 162(4): 921-931.

[4] SRIKANT S, WAGNER J L, VALDIVIA A, et al. Unstart detection in a simplified-geometry hypersonic inlet-isolator flow[J]. Journal of Propulsion and Power, 2010, 26(5): 1059-1071.

[5] CHANG J T, WANG L, QIN B, et al. Real-time unstart prediction and detection of hypersonic inlet based on recursive Fourier transform[J]. Proceedings of the Institution of Mechanical Engineers—Part G: Journal of Aerospace Engineering, 2015, 229(4): 772-778.

[6] MACMARTIN D G. Dynamics and control of shock motion in a near-isentropic inlet[J]. Journal of Aircraft, 2004, 41(4): 846-853.

[7] VALDIVIA A, YUCEIL K B, WAGNER J L, et al. Control of supersonic inlet-isolator unstart using active and passive vortex generators[J]. AIAA Journal, 2014, 52(6): 1207-1218.

[8] BAO W, LI B, CHANG J T, et al. Switching control of thrust regulation and inlet buzz protection for ducted rocket[J]. Acta Astronautica, 2010, 67(7/8): 764-773.

[9] LIU H K, YAN C, ZHAO Y T, et al. Active control method for restart performances of hypersonic inlets based on energy addition[J]. Aerospace Science and Technology, 2019, 85: 481-494.

[10] DOERFFER P P, BOHNING R. Shock wave-boundary layer interaction control by wall ventilation[J]. Aerospace Science and Technology, 2003, 7(6): 171-179.

[11] MOUNTS J S, BARBER T J. Numerical analysis of shock induced separation alleviation using vortex generators: AIAA Paper 1992-0751[R]. [S.l.]: AIAA, 1992.

[12] HOLDEN H A, BABINSKY H. Vortex generators near shock/boundary layer interactions: AIAA Paper 2004-1242[R]. [S.l.]: AIAA, 2004.

[13] TINDELL R H, WILLIS V P, Experimental investigation of blowing for controlling oblique shock/boundary layer interactions: AIAA Paper 1997-2642[R]. [S.l.]: AIAA, 1997.

[14] MACHERET S O, SHNEIDER M N, MILES R B. Scramjet inlet control by off-body energy addition: A virtual cowl[J]. AIAA Journal, 2004, 42(11): 2294-2302.

[15] KANTROWITZ A, DONALDSON C D. Preliminary investigation of supersonic diffusers: NACA ACR L5D20[R]. [S.l.]: NACA, 1945.

[16] VEILLARD X, TAHIR R, MOLDER S. Limiting contraction for starting simple ramp type scramjet intakes with overboard spillage[J]. Journal of Propulsion and Power, 2008, 24(5): 1042-1049.

[17] FALEMPIN F, WENDLING E, GOLDFELD M, et al. Experimental investigation of starting process for a variable geometry air inlet operating from Mach 2 to Mach 8: AIAA Paper 2006-4513[R]. [S.l.]: AIAA, 2006.

[18] DALLE D J, TORREZ S M, DRISCOLL J F. Performance analysis of variable-geometry scramjet inlets using a low-order model[C]//Proceedings of the 47th AIAA/ASME/SAE/ASEE Joint Propulsion Conference & Exhibit. San Diego, California: AIAA, 2011.

[19] TENG J, YUAN H. Variable geometry cowl sidewall for improving rectangular hypersonic inlet performance [J]. Aerospace Science and Technology, 2015, 42: 128-135.

[20] LIU Y, WANG L, QIAN Z S. Numerical investigation on the assistant restarting method of variable geometry for high Mach number inlet[J]. Aerospace Science and Technology, 2018, 79: 647-657.

[21] WANG J, XIE L, ZHAO H, et al. Fluidic control method for improving the self-starting ability of hypersonic inlets[J]. Journal of Propulsion and Power, 2016, 32(1): 1-8.

[22] HÄBERLE J, GÜLHAN A. Internal flow field investigation of a hypersonic inlet at Mach 6 with bleed[J].

Journal of Propulsion and Power, 2007, 23(5): 1007-1017.

[23] YUAN Huacheng, LIANG Dewang. Effect of suction on starting of hypersonic inlet[J]. Journal of Propulsion Technology, 2006, 27(6): 525-528. (in Chinese)

[24] CHANG J T, YU D R, BAO W, et al. Effects of boundary-layers bleeding on unstart/restart characteristics of hypersonic inlet[J]. The Aeronautical Journal, 2009, 113(1143): 319-327.

[25] LIU Z, LUO Z B, LIU Q, et al. Modulation of driving signals in flow control over an airfoil with synthetic jet[J]. Chinese Journal of Aeronautics, 2020, 33(12): 3138-3148.

[26] ASGARI E, TADJFAR M. Active control of flow over a rounded ramp by means of single and double adjacent rectangular synthetic jet actuators[J]. Computers and Fluids, 2019, 190: 98-113.

[27] GORTON S, OWENS L, JENKINS L, et al. Active flow control on a boundary-layer-ingesting inlet: AIAA Paper 2004-1203[R]. [S.l.]: AIAA, 2004.

[28] ALLAN B, OWENS L, BARRIE B. Numerical modeling of active flow control in a boundary layer ingesting offset inlet: AIAA Paper 2004-2318[R]. [S.l.]: AIAA, 2004.

[29] YOUNG D, JENKINS S A, MILLER D N. An investigation of active flowfield control for inlet shock/boundary layer interaction: AIAA Paper 2005-4020[R]. [S.l.]: AIAA, 2005.

[30] LUO Y H, LI J, LIANG H, et al. Suppressing unsteady motion of shock wave by high-frequency plasma synthetic jet[J]. Chinese Journal of Aeronautics, 2021, 34(9): 60-71.

[31] VAN WIE D M, KWOK F T, WALSH R T. Starting characteristics of supersonic inlets: AIAA Paper 1996-2914[R]. [S.l.]: AIAA, 1996.

[32] YOU Jin. Research on restarting characteristics and regulation methods of mix-compression inlet[D]. Changsha: National University of Defense Technology, 2016. (in Chinese)

[33] MENTER F R. Two-equation eddy-viscosity turbulence models for engineering applications[J]. AIAA Journal, 1994, 32(8): 1598-1605.

[34] ECONOMON T D, PALACIOS F, COPELAND S R, et al. SU2: An open-source suite for multi-physics simulation and design[J]. AIAA Journal, 2016, 54(3): 828-846.

[35] ROE P L. Approximate riemann solvers, parameter vectors, and difference schemes[J]. Journal of Computational Physics, 1981, 43(2): 357-372.

[36] VAN LEER B. Towards the ultimate conservative difference scheme V: A second order sequel to Godunov's method[J]. Journal of Computational Physics, 1979, 32(1): 101-136.

[37] YOON S, JAMESON A. Lower-upper symmetric-Gauss-Seidel method for the Euler and Navier-Stokes equations[J]. AIAA Journal, 1988, 26(9): 1025-1026.

[38] JAMESON A. Time dependent calculations using multigrid with applications to unsteady flows past airfoils and wing: AIAA Paper 1991-1596[R]. [S.l.]: AIAA, 1991.

[39] HÄBERLE J, GÜLHAN A. Investigation of two-dimensional scramjet inlet flowfield at Mach 7[J]. Journal of Propulsion and Power, 2008, 24(3): 446-459.

Acknowledgements The research was supported by the National Key Research and Development Program of China (No.2021YFA0719204), and the National Natural Science Foundation of China (No.12272387). The authors are also grateful to the National Supercomputer Center in Tianjin for providing the computational resource. Valuable suggestions given by Prof. YAN Chao in Beihang University are also acknowledged.

Authors Dr. **JIN Yichao** received the B.S. and M.S. degrees in mechanics from Beihang University, Beijing, China, in 2015 and 2018, respectively. He obtained Ph.D. degree in mechanics from University of Chinese Academy of Sciences in 2022. His research has focused on computational fluid dynamics, including hypersonic aerodynamics, supercritical fluid, and thermally-induced flow instability.

Prof. **YAO Wei** obtained Bachelor's and Master's engineering degrees from University of Science & Technology of China (USTC) in 2005 and 2007, respectively. He received his Ph.D. degree from University of Ulster (UU) in 2010. Prof. YAO joined Institute of Mechanics, Chinese Academy of Sciences (CAS) in 2013. His research interests include large eddy simulation of supersonic combustion, development and calibration of combustion models under scramjet conditions, reduced combustion kinetics relevant to engine fuels (e.g., Jet-A, RP-3, and hydrogen), numerical optimization of scramjets. Prof. YAO was awarded AIAA Best Hypersonic Systems and Technology Paper Award in 2018 and CAS Youth Innovation Promotion Association Award in 2019.

Author contributions Dr. **JIN Yichao** designed the study, performed the simulations, conducted the analysis, interpreted the results, and wrote the manuscript. Prof. **YAO Wei** contributed to the analysis, discussion, reviewing, and editing. All authors commented on the manuscript draft and approved the submission.

Competing interests The authors declare no competing interests.

(Production Editor: ZHANG Huangqun)

基于主动射流控制的高超声速进气道再起动性能研究

靳一超[1,2], 姚 卫[2,3]

(1.北京应用物理与计算数学研究所,北京 100094,中国; 2.中国科学院力学研究所高温气体动力学国家重点实验室,北京 100190, 中国; 3.中国科学院大学工程科学学院,北京 100049,中国)

摘要:基于主动射流技术,本文提出了一种应用于高超声速进气道再起动的控制方法。采用URANS(Unsteady Reynolds averaged Navier-Stokes)方法对再起动的动态过程进行了数值模拟,验证了控制方法的有效性,并揭示了射流条件的影响。主动射流将高压分离泡从内缩段转移至上游并充分膨胀,缓解了内缩段的逆压梯度,从而改善了进气道的不起动状态。关闭射流后,进气道在射流膨胀诱导的顺压环境中成功实现再起动。接着,分析了射流动量比的影响以指导射流控制方法的设计并选择合适的动量比。较低的射流动量不足以消除高压分离泡,而过大的射流动量则会诱导较强的弓形激波并造成严重的动量损失。移除射流后,将在下壁面形成较厚的低速层,使进气道回退为不起动状态。因此,使用主动射流辅助进气道再起动的一般原则为确保射流在出口下游充分膨胀,同时避免在上游造成较大的动量损失,并防止形成较厚的低速层。

关键词:高超声速进气道;不起动;再起动;主动射流;流动控制